CLINICAL ARTICLE

Mid- and Long-Term Follow-Up Efficacy Analysis of 3D-Printed Interbody Fusion Cages for Anterior Cervical Discectomy and Fusion

Yuan-zhang Jin, MM, Bin Zhao, MD, Xiang-dong Lu, MD, Yi-bo Zhao, MD, Xiao-feng Zhao, MD, Xiao-nan Wang, MM, Run-tian Zhou, MM, De-tai Qi, MM, Wen-xuan Wang, MD

Department of Orthopaedics, The Second Hospital of Shanxi Medical University, Taiyuan, China

Objective: To evaluate the safety and stability of 3D-printed interbody fusion cages (3D-printed cages) in anterior cervical discectomy and fusion (ACDF) by investigating the mid- and long-term follow-up outcomes.

Methods: In this prospective study, the clinical data of 30 patients with CSM admitted to the Second Hospital of Shanxi Medical University from May 2012 to May 2014 were analyzed. The cohort comprised 18 males and 12 females with an average age of 60.22 ± 3.2 years. All patients were examined by X-ray, CT and MRI before the operation. A total of 30 cases of CSM were treated by ACDF with 3D printed cage implantation. Mid- and long-term follow-ups were performed after the surgery. Clinical efficacy was evaluated by comparing the JOA score, SF-36 score, change in neurological function, cervical curvature index (CCI), vertebral intervertebral height (VIH) and fusion rate before the operation, 6 months after the operation, and at the last follow-up.

Results: Two of the 30 patients were lost to follow-up. The remaining patients were followed up for 48–76 (65.23 ± 3.54) months. The patients recovered satisfactorily with a significant clinical effect. The JOA score increased meanfully and the improvement rate was 89.4% at the final follow-up. The SF-36 score increased significantly from pre- to postoperatively. The height of the intervertebral space at the last follow-up was not statistically significantly different from that at 6 months after surgery ($P > 0.05$), showing that the height of the intervertebral space did not change much and the severity of cage subsidence (CS) decreased. The CCI improved from pre- to postoperatively. The CCI did not change much from the 6-month follow-up to the last follow-up. and the cage rate (CR) was 100% at the 6-month and last follow-ups. No severe complications, such as spinal cord injury, esophageal fistula, cerebrospinal fluid leakage, cervical hematoma or wound infection, occurred in any of the patients.

Conclusion: The clinical and radiological results show that the application of 3D-printed cages in ACDF can significantly relieve symptoms. Moreover, 3D-printed cages can restore the curvature of the cervical spine, effectively maintain the intervertebral height for a long time, and prevent complications related to postoperative subsidence.

Key words: ACDF; 3D printed cage; Mid- and long-term follow-up; Efficacy analysis

Introduction

Ossification of the cervical posterior longitudinal ligament and cervical disc herniation caused by cervical degeneration are common diseases of the spine. For individuals with severe symptoms and for whom conservative treatment is ineffective, surgery is the most direct and efficient treatment[1]. Among other surgeries, anterior cervical spine surgery is relatively less traumatic. It can be used to directly resect the

diseased intervertebral disc and osteophyte behind the vertebral body and relieve the pressure on the posterior spinal cord by direct decompression, thereby achieving complete decompression [2]. Simultaneously, it ensures satisfactory bone fusion, a normal intervertebral height, a physiological curvature, and cervical vertebral stability. Cloward[3] and Smith and Robinson[4] were the first to use anterior cervical discectomy and fusion (ACDF) to treat cervical degenerative diseases. After several years of development, ACDF has become the classic technique for anterior cervical surgery. Additionally, ACDF has achieved optimal clinical results, such as a good cervical fusion rate and strong internal fixation.

For the grafts used in ACDF, iliac crest autografts are still the gold standard, but donor site complications such as infection, pain and fracture are prone to occur. To reduce complications at the donor site, allogeneic bone grafts instead of iliac crest autologous bone grafts have been used more recently[5, 6]. However, there are some problems with allogeneic bone; that is, the probability of subsidence, collapse and nonunion is higher. It has been reported that the incidence of collapse ranges from 5% to 62.5% when allografts are used in ACDF[7–9].

More recently, interbody fusion cages have been used. These cages can shorten the hospitalization time, reduce the complications of transplantation and accelerate recovery[10]. At present, the most widely used cage materials are titanium alloy and polyether ether ketone (PEEK). The advantages of titanium alloy cages are the excellent levels of corrosion resistance, compression resistance and biocompatibility; the disadvantage is that the elastic modulus is relatively high, which may produce a stress shielding effect. A stress shielding effect occurs when the Young's moduli of the implant device and the bone are different, and stress is not transmitted between the implant device and the bone uniformly. The stress shielding effect leads to subsidence and even displacement of the cage when titanium alloy is used. The PEEK cage has the advantages of X-ray transmission, good biocompatibility and an elastic modulus equivalent to that of bone[11]. However, it also has disadvantages: the hydrophobic layer on its surface cannot be adsorbed by proteins or cells[12], so a firm bone-fusion cage interface cannot be formed, which affects the efficiency and effect of fusion and leads to cage subsidence and displacement.

Glibson et al. found that metals with porous structures can significantly decrease the Young's modulus. These metals seem to have the advantages of both titanium alloy and PEEK but not the respective disadvantages.

The 3D-printed models were based on the digital models. Plastic or powder metal materials were used to construct objects by "layered manufacturing, layer-by-layer superimposition" technology[13]. At present, in the medical field, it is also possible to manufacture ergonomically shaped objects through this rapid manufacturing, high-precision and customized production method[14]. This method has the advantages of precise, time-saving, and individualized treatment[15, 16]. With

the continuous development and advancement of 3D printing technology in the medical field, in recent years, 3D printing has been increasingly used in orthopedics[17]. It has been widely used in the reconstruction of bone defects[18–20], revision arthroplasty[21], spinal surgery[22], and the treatment of complex fractures[23]. 3D printing technology can be used to produce prostheses with precise bone defect contours. It also promotes bone growth in the trabecular hole at the bone-implant interface, which can promote osseointegration and reduce the long-term implant failure rate[24, 25]. When applied in cervical spine surgery, this technology can not only achieve more precise treatment but also maximize the physiological function of the cervical spine[26]. Generally, 3D-printed titanium cages have good osteogenic induction performance, and the pore structure allows the cages to promote osteoblast growth and adherence to the material surface[27]. Due to the porous structure, 3D-printed titanium cages are expected to induce osteogenesis and exhibit an even coating. Therefore, we used a new 3D-printed porous titanium interbody fusion cage, which is expected to simulate the biomechanical properties of bone minimize stress shielding and subsidence[28].

Herein, we analyzed the clinical data of 30 patients with cervical spondylotic myelopathy (CSM) treated by anterior cervical discectomy, 3D printing cage implantation, and titanium plate internal fixation in a prospective study. Moreover, mid- and long-term follow-ups were conducted to evaluate the clinical efficacy and imaging outcomes of these methods.

Data and Methods

Clinical Information
The current clinical research program was performed according to the Helsinki Declaration and approved by the Ethics Review Committee of the Second Hospital of Shanxi Medical University (2018LL039). All participants signed informed consent forms prior to participation in this study.

Patient information was collected prospectively according to the inclusion and exclusion criteria. A total of 30 patients (18 males and 12 females) with CSM were treated by anterior cervical discectomy, 3D printing cage implantation, and titanium plate internal fixation in the Second Affiliated Hospital of Shanxi Medical University in Taiyuan, China, from May 2012–2014. The age of the cohort ranged from 52–67 years, with an average of 60.22 ± 3.2 years. There were 26 cases of single-segment CSM: two cases at the C_{3-4} segment, 14 cases at the C_{4-5} segment, seven cases at the C_{5-6} segment, and three cases at the C_{6-7} segment. There were four cases of double-segment CSM: one case of CSM at the C_{3-4} and C_{4-5} segments, two cases at the C_{4-5} and C_{5-6} segments, and one case at the C_{5-6} and C_{6-7} segments. Regarding the preoperative symptoms and signs of CSM, limb numbness and weakness were found in 30 cases (100%), pathological signs were found in 16 cases (53.33%), and limb muscle tension was found in 19 cases (63.33%).

The inclusion criteria were: (i) CSM; (ii) planning to undergo a surgical approach suitable for ACDF; and (iii) an age ≥ 18 years.

The exclusion criteria were as follows: (i) complications including cervical vertebral fractures, tumors, or infections; (ii) nervous system diseases; (iii) immunosuppressive diseases; and (iv) poor cardiopulmonary function or intolerance to surgical stimulation.

General Information

The 3D-printed cage was created with titanium alloy powder by electron beam machining (EMB). The overall structure was a black-gray wedge-shaped structure with a porosity of 80% and a pore size of 800 ± 200 μm. Its overall shape was wedge-shaped (viewed from the side), and its upper top surface, which was the surface that made contact with the lower endplate of the upper vertebral body, was arc-shaped to increase the contact area. This wedge-shaped structure was designed with three lordosis angles to correct the curvature of the entire vertebral body: $0°$, $4°$ and $8°$. The left and right diameters were 15 mm and 17 mm; the front and rear diameters were 12.5 mm and 14 mm. There were seven heights, ranging from 4–10 mm and increasing in increments of 1 mm. There was a reserved bone graft window in the center, which was designed to be used when bone grafting was required under special circumstances (Fig. 1).

Evaluation Criteria and Follow-up

All the patients were examined by X-ray, computed tomography (CT), and magnetic resonance imaging (MRI) preoperatively, 6 months after the operation, and at the last follow-up. All the patients were followed up after the operation.

The JOA was used to assess the following four aspects of spinal cord function: motor function of the upper limbs, motor function of the lower limbs, sensation of the limbs and trunk, and bladder function[29]. The highest score was 17 points, which indicated normal function, and the lower the score was, the more obvious the dysfunction. This is a reliable, validated assessment tool[30], and the results are consistent with psychometric characteristics[31].

The JOA score was recorded preoperatively, at 6 months after the operation and at the last follow-up. The rate of improvement in the JOA score was calculated as follows according to the results of the last follow-up: improvement rate = (last follow-up JOA score - preoperative JOA score) / (17 - preoperative JOA score) × 100%, i.e., improvement rate = (improvement score/loss score) × 100%. The rate of improvement was categorized as follows: an improvement rate ≥ 80% was excellent; an improvement rate ≥ 50% was good; and a rate < 50% was bad.

The SF-36 Score Was Used to Assess Each Patient's General Health Status

The SF-36 concise health questionnaire comprehensively summarizes the quality of life of the surveyed participants regarding eight aspects: physiological function, physiological function, body pain, general health, energy, social function, emotional function and mental health.

The SF-36 score is widely used to determine the quality of life of individuals in the general population.

Neurological Function was Assessed Qualitatively Using Odom's Criteria

The level of neurological function was considered excellent when no relevant cervical spondylosis symptoms were observed and the patient could carry out their daily work; good when there was occasional discomfort, but the symptoms did not affect the patient's ability to perform daily work; moderate when the symptoms of cervical spondylosis improved but affected the patients ability to perform daily work; and poor when there was no improvement and the condition worsened.

The cervical curvature index (CCI) was calculated using the Ishihara method to evaluate the cervical curvature[32]. Line A of the inferior posterior angle of the C_2 vertebra and the posterior inferior angle of the C_7 vertebra was deduced on the cervical lateral radiographs. The vertical lines of connection A were made from the posterior and inferior angles of the C_3, C_4, C_5, and C_6 vertebral bodies. Lines a1, a2, a3, and a4 were identified. The lengths of the above lines were measured. Values to the left side of the vertical line were considered positive, and those to the right side were negative (Fig. 2). CCI = $100 \times (a1 + A2 + a3 + a4) / A$.

For the vertebral disk height, as shown in Fig. 3, the distance between the midpoint of the upper endplate of the fused segment and the midpoint of the lower endplate of the fused segment was measured on the lateral cervical radiograph.

For the cage fusion rate, according to the FDA and Kandziora criteria, the fusion status of the cervical fusion cage with the titanium plate and screw internal fixation system was evaluated. The fusion conditions with bone grafts that fulfilled the following conditions were considered fused; otherwise, the cases were considered nonfused.

1. X-ray taken in the cervical flexion-extension dynamic position showed that the angle of the fusion intervertebral body changed by <5°.

Fig. 1 3D-printed cage.
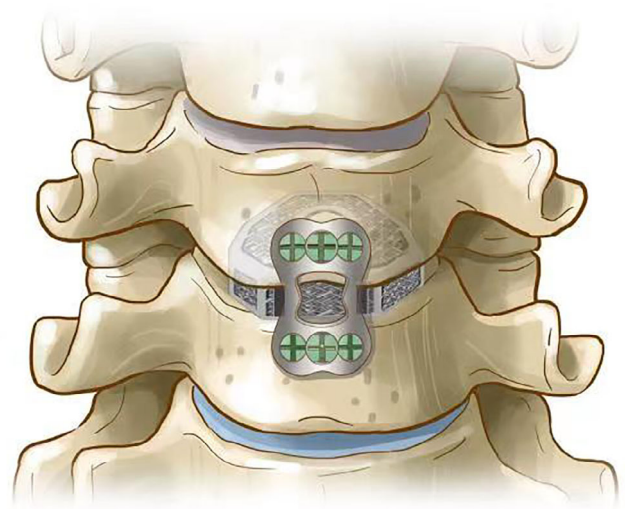
Fig. 2 Cervical curvature (Ishihara method).

Fig. 4 The working principle of the 3D printed cage (coronal plane).

Fig. 3 Intervertebral height of the fused segment.

Fig. 5 The working principle of the 3D printed cage (sagittal plane).
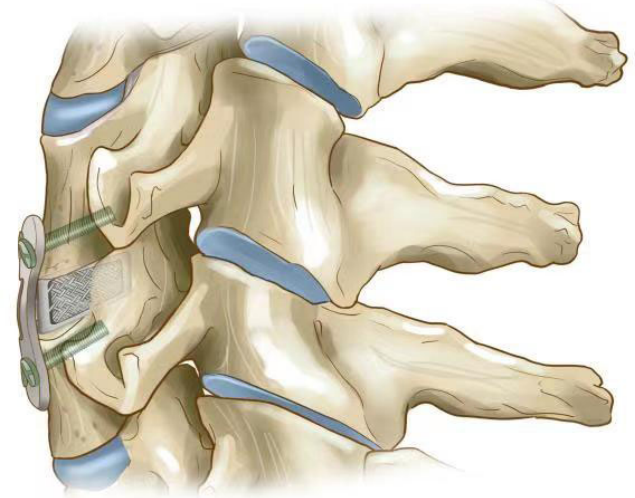
2. No obvious translucent bands around the fuser or displacement were detected.
3. The titanium plate screw system did not loosen, and the surrounding bone transparent area was <50% of its surrounding surface.

Surgical Methods

The patient was placed in a supine position with slight neck extension and was administered general anesthesia. A transverse incision of the right neck was made between the thyroid cartilage and the cricoid cartilage. The lesions were exposed layer by layer. C-arm X-ray was used to located the lesion segment. The diseased intervertebral discs were excised, the upper and lower vertebrae were distracted by the distractor, and the osteophytes on the posterior margin of the vertebral body were removed from the posterior longitudinal ligament. The cartilage tissue adjacent to the endplate was scraped, leading to osseous bleeding, and the 3D-printed cage was selected to be fixed in the lesion responsibility space. The appropriate anterior cervical titanium plate was selected, and four screws were placed sequentially. The position and depth of the titanium plate and screw were assessed by C-arm fluoroscopy, thorough rinsing was performed, an indwelling drainage tube was placed, the wound was closed layer by layer, and the operation was completed (Figs 4 and 5).

TABLE 1 Follow-up data for each group

Indexes	Preoperative assessment	Six-month follow-up	Last follow-up
JOA score	9.78 ± 0.96	16.13 ± 0.72	16.47 ± 0.61
SF-36 score	524.8 ± 10.8	655.5 ± 8.89	660.8 ± 8.92
Cervical curvature (°)	10.08 ± 1.21	13.65 ± 1.03	13.51 ± 0.86
Intervertebral pace height (mm)	35.58 ± 0.85	37.15 ± 1.23	36.9 ± 0.73
Cage fusion rate	-	100%	100%

Statistical Analysis

The data were analyzed by SPSS 19.0 (SPSS Inc., Chicago, IL), and the quantitative data are expressed as ($\bar{x} \pm s$). The quantitative data included the JOA score, SF-36 score, Odom's standard for nerve function, cervical curvature and intervertebral space height before surgery, at the 6-month follow-up and at the last follow-up. The three groups of data were compared and analyzed by the single factor repeated measures variance analysis method. The qualitative data on neurological function, regarding Odom's standard grading system, recorded before surgery, at the 6-month follow-up and at the final follow-up were compared using the Kruskal-Wallis H rank-sum test. The significance level α was 0.05 (Fig. 6).

Results

Surgery Situation

The operation was performed successfully in all 30 patients. The operation time was 50–80 (average, 60.50 ± 3.25) min, and the bleeding volume was 40–70 (average, 50.35 ± 4.27) mL. The symptoms of cervical spondylosis significantly improved in all patients. No severe complications, such as spinal cord injury, esophageal fistula, neck hematoma, wound infection or cerebrospinal fluid leakage, occurred in any of the patients (Fig. 7).

Follow-up Data

All patients were followed up every 3 months in the first year, every 6 months in the second year, and every year thereafter. Two patients were completely lost to follow-up at 6 months after the operation, and the remaining 28 were followed up for 48–76 (average, 65.23 ± 3.54) months. The follow-up period is still ongoing (Fig. 8).

Cervical Curvature Index

There was a significant main effect of the time point on the total curvature of the cervical vertebra ($F = 38.71$, $P < 0.001$). The CCI changed significantly from 10.08 ± 1.21 preoperatively to 13.65 ± 1.0 at 6 months after the operation ($t = 39.84$, $P < 0.05$). The CCI value at the last follow-up (13.51 ± 0.86) was significantly different from the preoperative value ($t = 36.74$, $P < 0.05$), but no significant differences were detected between the 6-month

TABLE 2 Neurological function Odom's criteria

Time	Excellent	Good	Poor	Bad
Preoperatively	0	10	14	4
Six-month follow-up	15	7	6	0
The last follow-up	17	8	3	0

JOA scores; There as a significant main effect of the time point, including the preoperative, 6-month follow-up and last follow-up time points, on.

follow-up and either of the other time points ($t = 2.59$, $P > 0.05$) (Table 1).

Vertebral Disk Height

There was a significant main effect of the time point on the vertebral intervertebral height ($F = 79.49$, $P < 0.001$). The height of the intervertebral space recovered from 35.58 ± 0.85 preoperatively to 37.15 ± 1.23 at 6 months after the operation and 36.95 ± 0.73 at the last follow-up. The height of the intervertebral space at 6 months after the operation was significantly higher than that before the operation ($P < 0.001$). A significant difference was observed between the last follow-up and the preoperative assessment ($P < 0.001$), while no significant differences were detected between the last follow-up and that at 6 months after the operation ($P > 0.05$) (Table 2).

Odom Criteria for Neurological Function

There were significant differences across the preoperative assessment, 6-month follow-up and final follow-up in neurological function according to Odom's standard grading system ($\chi^2 = 433.33$, $P < 0.05$) (Table 2). At 6 months after the operation and at the last follow-up, significant improvements occurred with respect to before the operation ($\chi^2 = 20.868$, $P < 0.05$), while no significant differences were detected between the last follow-up and that at 6 months after the operation ($\chi^2 = 3.501$, $P > 0.05$).

Cage Fusion Rate

According to cervical X-ray findings, the cage fusion rate was 100% at the 6-month and the last follow-ups.

Case 1: Fig. 6.

MIS- AND LONG-TERM FOLLOW-UP EFFICACY ANALYSIS
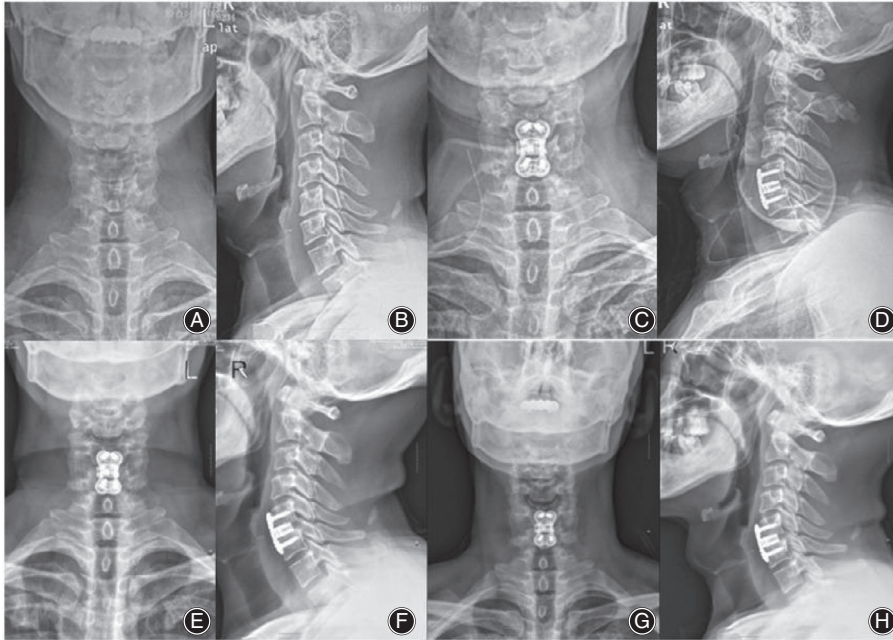
Fig. 6 The patient was a 63-year-old male with C$_{5-6}$ segment disc herniation. The limbs were numb and weak before the operation, fine movements were difficult to complete with either hand, and the Babinski and Hoffmann sign test results were positive. The patient gradually recovered muscle strength after the operation, and the symptoms were relieved with respect to before the operation. A, B The preoperative X-ray is shown, C, D the postoperative X-ray is shown, E, F the C$_{5-6}$ segments were fused at 6 months after the operation, G, H the cage was well positioned, no loosening or breaking of titanium plate screw was found, and the fusion status was firm at 68 months after the operation.

Case 2: Fig. 7.
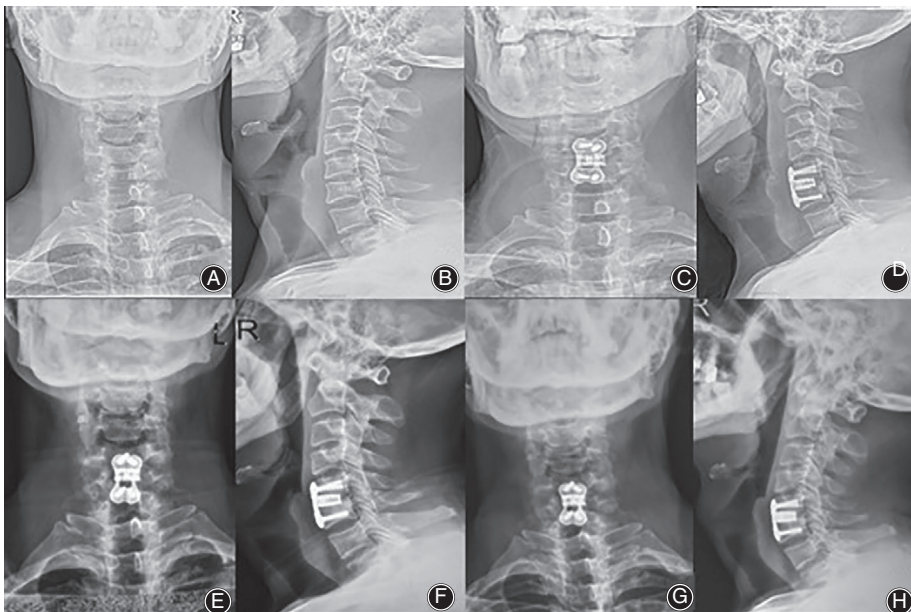
Fig. 7 The patient was a 58-year-old male with C$_{5-6}$ cervical disc herniation. A, B The X-ray before the operation is shown, and C, D the postoperative X-ray is shown. E, F Six months after the operation, C$_{5-6}$ was fused, and G, H 72 months after the operation, there was no loosening or prolapse of internal fixation.

Case 3: Fig. 8.
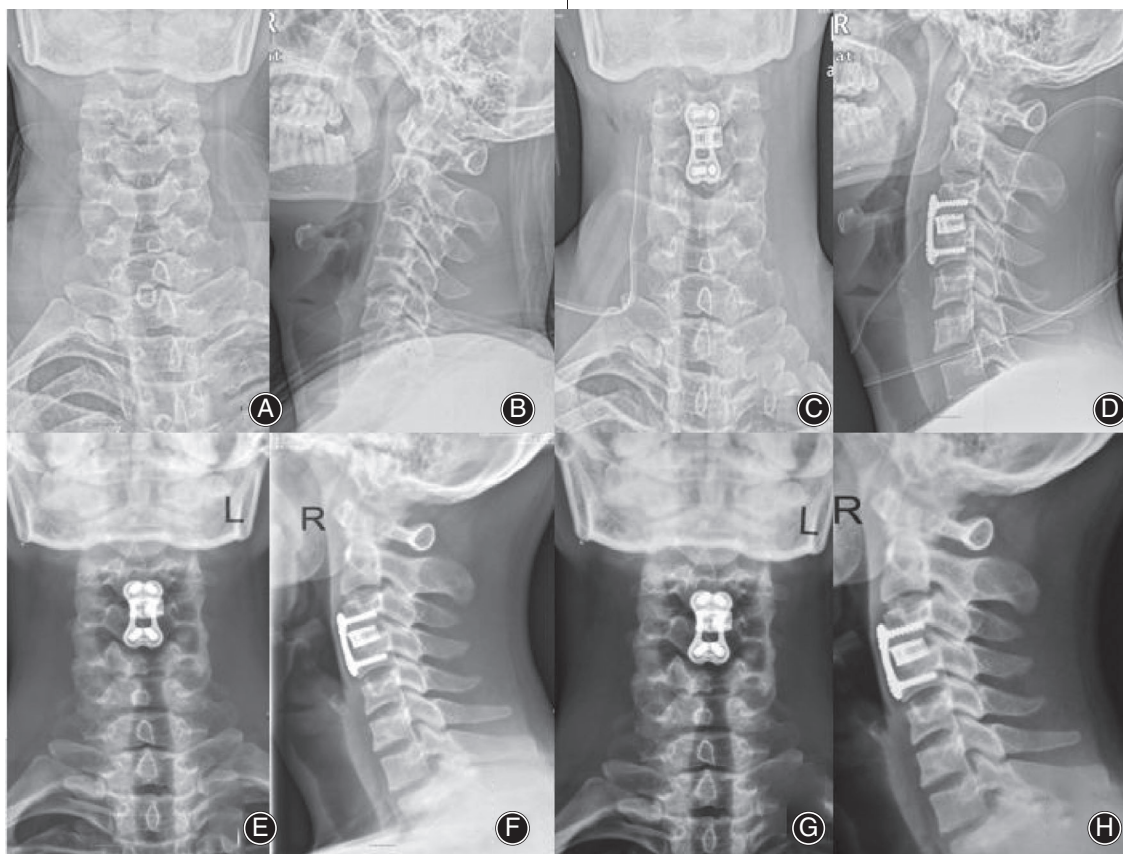
Fig. 8 The patient was a 60-year-old male with CSM (C_{3-4}). A, B The X-ray before the operation is shown, and C, D the postoperative X-ray is shown. E, F Six months after the operation, C_{5-6} was fused, and G, H 72 months after the operation, there was no loosening or prolapse of internal fixation.

Discussion

ACDF has become the standard treatment for degenerative cervical disc disease. ACDF can restore the height of the intervertebral space, as a cage that promotes fusion of the adjacent vertebral bodies by the "stretching-compressing tension band" effect is inserted. Cage implantation reduces the loss of intervertebral height, reduces the occurrence of intervertebral foramen stenosis, promotes the recovery of the physiological cervical curvature, preserves cervical lordosis, avoids cervical kyphosis deformities, reduces the pressure on the spinal cord and nerve root, and prevents the degeneration of adjacent segments[33].

The ideal cage implant is biocompatible and has sufficient physical and mechanical properties[34]. In this context, we can conclude that 3D printing technology is a promising method and is one of most suitable methods to make cages to replace natural tissues in terms of function and structure. Moreover, 3D-printed cages are three-dimensional porous structures that are made of titanium alloy powder, with a porosity of 80% and a pore size of 800 ± 200 μm, and have a bone-like trabecular structure. This structure can not only

have an elastic modulus equivalent to that of human cancellous bone, reduce the stress shielding effect, and improve the intervertebral fusion rate but also allow bone cells to grow into it, forming a hinge between the bone and the implant and enhancing the connection between the bone bed and the implant[35, 36]. While the porous structure design effectively reduces the elastic modulus of the material, the compressive strength also decreases accordingly. Since the mechanical strength and fatigue strength of the implants that are used as load-bearing parts for a long time are equally important, the mechanical strength and fatigue performance of this porous cage may be of concern. Stamp et al.[33] once proposed that to achieve bone tissue ingrowth, the porosity of the implant material should be greater than 65%, the elastic modulus should be less than 3 GPa, and the compressive strength should not be less than 50 MPa. Ramulu et al.[34] found that the fatigue strength of 3D printed Ti-6Al-4V alloy bulk material is very high. Li et al.[37] fabricated 3D printed porous Ti-6Al-4V with porosities between 60% and 85% by the EBM method to study its fatigue strength and found that the fatigue index factor of 3D-printed regular Ti-6Al-4V porous

materials was twice that of random porous materials. This finding shows that 3D printing is an ideal method for processing porous materials. Yin et al.[36] found that in terms of mechanical testing, 3D-printed cages are superior to traditional intervertebral fusion cages, which further verifies that 3D-printed cages have good stability in cervical fusion surgery.

Another important factor that promotes fusion is the rough surface of the 3D-printed cage, which is created by melting Ti6Al4V particles. Compared with the smooth titanium surface, the rough surface is more conducive to cell adhesion[37, 38]. The cell adhesion rate is an important indicator for studying the early biocompatibility of implants. Strong adhesion can lead to rapid cell sedimentation and fast differentiation, which promote osseointegration[39–41].

A previous study showed[42] that the size, shape, structure, and surface coating of the cages considerably affect the efficiency and effectiveness of spinal fusion. Kim et al.[43]. speculated that the protruding structure of the head side of the cage increases the contact area with the endplate such that the intervertebral stress can be uniformly transferred and distributed on the cage, thereby promoting the growth of bone tissue and the fusion of adjacent segments. The curved surface was designed so that the upper surface of the 3D printed cage made contact with the endplate. This curved surface design increases the area of contact with the upper endplate, promotes fusion between the vertebral bodies and ensures intervertebral stability.

The left and right diameters were 15 mm and 17 mm, and the anterior and posterior diameters were 12.5 mm and 14 mm the JOA score ($F = 433.33$, $P < 0.001$). The JOA score at 6 months after the operation was significantly different from that before the operation ($t = 96.32$, $P < 0.05$). Additionally, a significant difference was observed between the JOA score at the last follow-up and the preoperative JOA score ($t = 96.32$, $P < 0.05$), while no significant difference was detected between the last follow-up and the 6-month follow-up ($t = 0.243$, $P > 0.05$). The rate of improvement in the JOA score was 92.7%. At the last follow-up, the rate of improvement rate in the JOA score was excellent in 24 cases, good in five cases, and bad in one case.

SF-36 Score

There was a significant main effect of the time point on the SF-36 score ($F = 1534.35$, $P < 0.001$). The SF-36 score at 6 months after the operation was significantly higher than that before the operation ($t = 1072.18$, $P < 0.05$). A significant difference in the score was detected between the last follow-up after and before the operation ($t = 1181.66$, $P < 0.05$). No significant differences were observed between the last follow-up and 6-month follow-up ($t = 74.18$, $P > 0.05$). A variety of cage specifications can be used to match the specifications of an individual vertebral body to the greatest extent. These specifications maximize the contact area and produces a uniform stress distribution.

Studies have shown that maximizing the area of the bone-hardware interface can minimize stress shielding and cage subsidence. Serra et al.[43] conducted the endplate matching test and showed that 3D-printed cages were superior to other cages in terms of compatibility with the cervical endplate, indicating that 3D-printed cages yield better fixation stability.

Cage subsidence occurs when the cage enters the vertebral body with a relatively low elastic modulus. Cage subsidence is inevitable after ACDF. Fujibayashi et al.[44] suggested that there was 1–2 mm subsidence in the early stage after anterior cervical surgery. Most cage subsidence cases occurred in the posterior part of the vertebral body. Slight subsidence can help restore the angle of cervical lordosis. According to a previous study, slight subsidence may improve the fusion rate and cervical curvature[45]. Since cage subsidence compromises the intervertebral height, excessive subsidence may lead to subsidence-related complications, such as cervical kyphosis, the recurrence of neurological symptoms, and internal fixation failure[46–49]. Lee et al.[50] studied patients who underwent single-segment ACDF and suggested that subsidence mostly occurred within half a year after the operation. Afterwards, due to the stability of interbody fusion, the settlement usually did not continue to progress, and the occurrence of subsidence had a negative impact on sagittal parameters and the clinical prognosis. Wu et al.[51] reported that there is no significant correlation between subsidence and the clinical prognosis and that the clinical effect mainly depends on the magnitude of improvement in cervical lordosis. Most scholars use 3 mm as the threshold for subsidence[52, 53]. In this study, intervertebral cage subsidence (CR) was defined as a decrease in intervertebral space height.

The height of the intervertebral space recovered from 35.58 ± 0.85 mm preoperatively to 37.15 ± 1.23 mm at the 6-month follow-up and 36.95 ± 0.73 mm at the last follow-up. The results showed that the height of the intervertebral space significantly improved from pre- to postoperatively, and no cases of significant cage settlement were found at the mid- or long-term follow-ups. There was only slight subsidence.

Among the factors that affect settlement, excessive scraping of the endplate during surgical operations is an important factor. Lim et al.[54] found that the average compressive yield load of the intact endplate was 634 N. When the end plate was partially removed, the average compressive yield load decreased to 494 N, and after the end plate was completely removed, the average compressive yield load decreased further to 419 N. Therefore, to provide enough compressive strength to resist subsidence, the osteogenic endplate should be carefully preserved while the cartilage endplate is completely scraped during the operation, and the 3D-printed cage has some unique advantages. Studies evaluating the geometry of the cervical endplate have shown that the upper endplate is tilted, while the lower endplate is mostly depresse[47, 55].

3D-printed cages are wedge-shaped, and the top surface is curved, which greatly increases the contact area and produces a uniform stress distribution, thus ensuring the recovery of cervical lordosis and preventing severe subsidence.

MIS- AND LONG-TERM FOLLOW-UP EFFICACY ANALYSIS

In the patients who received the 3D-printed cage, fusion occurred at 6 months after surgery. There are several reasons to promote the use of these cages: (i) the elastic modulus is low; (ii) the porous structure can be used for bone growth; (iii) the contact area is large and relatively matched; and (iv) the surface is coated with BMP osteoinductive coating.

Cervical lordosis is widely recognized as a normal manifestation. Kyphosis is closely related to cervical spondylosis. When the cervical spine is balanced in the sagittal plane, the individual can maintain an upright posture and horizontal field of vision with minimal energy consumption[56, 57]. The wedge shape of the cage can promote the recovery of the cervical spine curvature. The three lordosis angles of 0°, 4° and 8° are used so that cages with different anteversion angles are available for different surgical segments, thereby promoting the recovery of the angle of cervical spine lordosis. The CCI changed from 10.08 ± 1.21 preoperatively to 13.65 ± 1.03 at the 6-month follow up and 13.51 ± 0.86 at the last follow-up, indicating that the surgery can significantly improve cervical curvature. After the mid- and long-term follow-ups, we did not find any significant changes in cervical curvature.

Moreover, 3D-printed cages can eliminate the need for the bone grafting step, thereby shortening the operation time, reducing the difficulty of surgery, and reducing the risk of surgical complications associated with humeral bone removal. On the other hand, the surface BMP osteoinductive coating can also promote intervertebral fusion and potentially spine stability.

In the present study, 28 patients returned to normal living conditions at the last follow-up. The JOA score at the last follow-up was as high as 16.47 ± 0.61, and the rate of improvement in the JOA score at the last follow-up was 92.7%. The SF-36 score at the final follow-up was 660.8 ± 8.92 points. According to Odom's criteria, the neurological functional status significantly improved at the 6-month and last follow-ups compared with preoperatively. The above results indicated that the patients recovered satisfactorily. The height of the intervertebral space recovered from 35.58 ± 0.85 mm preoperatively to 37.15 ± 1.23 mm at the 6-month follow-up and 36.95 ± 0.73 mm at the final follow-up. The results showed that the height of the intervertebral space significantly improved from pre- to postoperatively, and no cases of cage settlement were found after the mid- and long-term follow-ups. In addition, according to the X-ray findings at the last follow-up, no cases of loosening of the titanium plate and screw or clear zones around the fusion cage were observed, while the adjacent segments in all patients had been fused.

In this study, clinical and radiological results show that 3D-printed cages in ACDF can significantly relieve symptoms. Moreover, 3D-printed cages can restore the curvature of the cervical spine, effectively preserve the intervertebral height for a long time, and prevent complications related to postoperative subsidence.

Based on the above follow-up results, we believe that the application of 3D-printed cages in ACDF is safe and stable. However, since the results of this study were not compared with those of the traditional cages used in ACDF, this study has some limitations.

References

1. Parkinson JF, Sekhon LHS. Cervical arthroplasty complicated by delayed spontaneous fusion: case report. J Neurosurg Spine, 2005, 2: 377–380.
2. Cloward RB. The anterior approach for removal of ruptured cervical disks 1958. J Neurosurg Spine, 2007, 6: 496–511.
3. Smith GW, Robinson RA. The treatment of certain cervical-spine disorders by anterior removal of the intervertebral disc and interbody fusion. J Bone Joint Surg Am, 1958, 40: 607–624.
4. Shriver MF, Lewis DJ, Kshettry VR, Rosenbaum BP, Benzel EC, Mroz TE. Pseudoarthrosis rates in anterior cervical discectomy and fusion: a meta-analysis. Spine J, 2015, 15: 2016–2027.
5. Yue WM, Brodner W, Highland TR. Long-term results after anterior cervical discectomy and fusion with allograft and plating: a 5- to 11-year radiologic and clinical follow-up study. Spine (Phila Pa 1976), 2005, 30: 2138–2144.
6. Martin GJ et al. Anterior cervical discectomy with freeze-dried fibula allograft. Spine(Phila Pa 1976), 1999, 24: 852–859.
7. Song KJ, Choi BY. Current concepts of anterior cervical discectomy and fusion: a review of literature. Asian Spine J, 2014, 8: 531–539.
8. Ali G, Prashanth R, Richard F. Dynamic plates in anterior cervical fusion surgery: graft settling and cervical alignment. Spine(Phila Pa 1976), 2009, 34: 1567–1571.
9. Li Y, Wu ZG, Li XK, et al. A polycaprolactone-tricalcium phosphate composite scaffold as an autograft-free spinal fusion cage in a sheep model. Biomaterials, 2014, 35: 5647–5659.
10. Greg Anderson D, Albert TJ. Bone grafting, implants, and plating options for anterior cervical fusions. Orthop Clin, 2002, 33: 317–328.
11. Simmons E. Anterior cervical discectomy and fusion. A clinical and biomechanical study with eight-year follow-up. J Bone Joint Surg Br, 1969, 51: 225–237.
12. Michalski MH, Ross JS. The shape of things to come. JAMA, 2014, 312: 2213–2214.
13. Brunello G, Sivolella S, Meneghello R, et al. Powder-based 3D printing for bone tissue engineering. Biotechnol Adv, 2016, 34: 740–753.
14. Malik HH, Darwood ARJ, Shaunak S, et al. Three-dimensional printing in surgery: a review of current surgical applications. J Surg Res, 2015, 199: 512–522.
15. Mulford J, Mackay N, Babazadeh S. Three dimensional printing in Orthopaedic surgery: a review of current and future applications. Orthop J Sports Med, 2016, 4: 2325967116S00022.
16. Cavanaugh PK, Mounts T, Vaccaro AR. Use of 3-dimensional printing in spine care. Contemp Spine Surg, 2015, 16: 1–5.
17. Liang H, Ji T, Zhang Y, Wang Y, Guo W. Reconstruction with 3D-printed pelvic endoprostheses after resection of a pelvic tumour. Bone Joint J, 2017, 99: 267–275.
18. Wei R, Guo W, Ji T, Zhang Y, Liang H. One-step reconstruction with a 3D-printed, custom-made prosthesis after total en bloc sacrectomy: a technical note. Eur Spine J, 2017, 26: 1902–1909.
19. Faizan A, Bhowmik-Stoker M, Alipit V, et al. Development and verification of novel porous titanium Metaphyseal cones for revision total knee athroplasty. J Arthroplasty, 2017, 32: 1946–1953.
20. Spetzger U, Frasca M, König SA. Surgical planning, manufacturing and implantation of an individualized cervical fusion titanium cage using patient-specific data. Eur Spine J, 2016, 25: 2239–2246.
21. Adams SB et al. Salvage of severe Foot and Ankle trauma with a 3D printed scaffold. Foot Ankle Int, 2016, 37: 433–439.
22. Macbarb RF, Lindsey DP, Bahney CS, Woods SA, Yerby SA. Fortifying the bone-implant Interface part 1: an in vitro evaluation of 3D-printed and TPS porous surfaces. Int J Spine Surg, 2017, 11: 105–115.
23. Shah FA, Omar O, Suska F, Snis A, Palmquist A. Long-term osseointegration of 3D printed CoCr constructs with an interconnected open-pore architecture prepared by electron beam melting. Acta Biomater, 2016, 36: 296–309.
24. Abdulhadi MA, Perno JR, Melhem ER, Nucifora PG. Characteristics of spondylotic myelopathy on 3D driven-equilibrium fast spin Echo and 2D fast spin Echo magnetic resonance imaging: a retrospective cross-sectional study. PLoS One, 2014, 9: e100964.
25. Bassous NJ, Jones CL, Webster TJ. 3-D printed Ti-6Al-4V scaffolds for supporting osteoblast and restricting bacterial functions without using drugs: predictive equations and experiments. Acta Biomater, 2019, 96: 662–673.
26. Association JO. Scoring system for cervical myelopathy. J Jpn Orthop Assoc, 1994, 68: 490–503.

27. Yonenobu K, Abumi K, Nagata K, Taketomi E, Ueyama K. Interobserver and intraobserver reliability of the japanese orthopaedic association scoring system for evaluation of cervical compression myelopathy. Spine(Phila Pa 1976), 2001, 26: 1890–1894.

28. Kato S, Oshima Y, Matsubayashi Y, Taniguchi Y, Tanaka S, Takeshita K. Minimum clinically important difference and patient acceptable symptom state of Japanese Orthopaedic association score in degenerative cervical myelopathy patients. Spine (Phila Pa 1976), 2019, 44: 691–697.

29. Takeshita K, Murakami M, Kobayashi A, Nakamura C. Relationship between cervical curvature index (Ishihara) and cervical spine angle (C2–7). J Orthop Sci, 2001, 6: 223–226.

30. Topuz K, Olak A, Kaya S, et al. Two-level contiguous cervical disc disease treated with peek cages packed with demineralized bone matrix: results of 3-year follow-up. Eur Spine J, 2009, 18: 238–243.

31. Palmquist A, Snis A, Emanuelsson L, Browne M, Thomsen P. Long-term biocompatibility and osseointegration of electron beam melted, free-form-fabricated solid and porous titanium alloy: experimental studies in sheep. J Biomater Appl, 2013, 27: 1003–1016.

32. Murr LE, Gaytan SM, Medina F, et al. Next-generation biomedical implants using additive manufacturing of complex, cellular and functional mesh arrays. Philos Trans R Soc, A, 2010, 368: 1999–2032.

33. Stamp R, Fox P, O'Neill W, Jones E, Sutcliffe C. The development of a scanning strategy for the manufacture of porous biomaterials by selective laser melting. J Mater Sci: Mater Med, 2009, 20: 1839–1848.

34. Ramulu M, Edwards P. Fatigue performance evaluation of selective laser melted Ti-6A1-4V. Mater Sci Eng, A, 2014, 598: 327–337.

35. Li SJ, Murr LE, Cheng XY, et al. Compression fatigue behavior of Ti–6Al–4V mesh arrays fabricated by electron beam melting. Acta Mater, 2012, 60: 793–802.

36. Yin X, Jiang L, Yang J, Cao L, Dong J. Application of biodegradable 3D-printed cage for cervical diseases via anterior cervical discectomy and fusion (ACDF): an in vitro biomechanical study. Biotechnol Lett, 2017, 39: 1433–1439.

37. Yang J, Cai H, Lv J, et al. In vivo study of a self-stabilizing artificial vertebral body fabricated by electron beam melting. Spine(Phila Pa 1976), 2014, 39: E486–E492.

38. Xue W, Krishna BV, Bandyopadhyay A, Bose S. Processing and biocompatibility evaluation of laser processed porous titanium. Acta Biomater, 2007, 3: 1007–1018.

39. Kawai T, Takemoto M, Fujibayashi S, et al. Comparison between alkali heat treatment and sprayed hydroxyapatite coating on thermally-sprayed rough Ti surface in rabbit model: effects on bone-bonding ability and osteoconductivity. J Biomed Mater Res, Part B, 2015, 103: 1069–1081.

40. Lv J, Jia Z, Li J, et al. Electron beam melting fabrication of porous Ti6Al4V scaffolds: cytocompatibility and osteogenesis. Adv Eng Mater, 2015, 17: 1391–1398.

41. Palissery V, Mulholland RC, Mcnally DS. The implications of stress patterns in the vertebral body under axial support of an artificial implant. Med Eng Phys, 2009, 31: 833–837.

42. Kim HS, Song JS, Heo W, Cha JH, Rhee DY. Comparative study between a curved and a wedge PEEK cage for single-level anterior cervical discectomy and Interbody fusion. Korean J Spine, 2012, 9: 181–186.

43. Serra T, Capelli C, Toumpaniari R, et al. Design and fabrication of 3D-printed anatomically shaped lumbar cage for intervertebral disc (IVD) degeneration treatment. Biofabrication, 2016, 8: 035001.

44. Fujibayashi S, Neo M, Nakamura T. Stand-alone interbody cage versus anterior cervical plate for treatment of cervical disc herniation: sequential changes in cage subsidence. J Clin Neurosci, 2008, 15: 1017–1022.

45. Jang JW, Lee JK, Lee JH, Hur H, Kim TW, Kim SH. Effect of posterior subsidence on cervical alignment after anterior cervical corpectomy and reconstruction using titanium mesh cages in degenerative cervical disease. J Clin Neurosci, 2014, 21: 1779–1785.

46. Chen Y, Chen D, Guo Y, et al. Subsidence of titanium mesh cage: a study based on 300 cases. J Spinal Disord Tech, 2008, 21: 489–492.

47. Jianxin W. Anatomy-related risk factors for the subsidence of titanium mesh cage in cervical reconstruction after one-level corpectomy. Int J Clin Exp med, 2015, 8: 7405–7411.

48. Yan D, Wang Z, Deng S, Li J, Soo C. Anterior corpectomy and reconstruction with titanium mesh cage and dynamic cervical plate for cervical spondylotic myelopathy in elderly osteoporosis patients. Arch Orthop Trauma Surg, 2011, 131: 1369–1374.

49. Fengbin Y, Jinhao M, Xinyuan L, Xinwei W, Yu C, Deyu C. Evaluation of a new type of titanium mesh cage versus the traditional titanium mesh cage for single-level, anterior cervical corpectomy and fusion. Eur Spine J, 2013, 22: 2891–2896.

50. Lee YS, Kim YB, Park SW. Risk factors for postoperative subsidence of single-level anterior cervical discectomy and fusion: the significance of the preoperative cervical alignment. Spine(Phila Pa 1976), 2014, 39: 1280–1287.

51. Wu WJ, Jiang LS, Liang Y, Dai LY. Cage subsidence does not, but cervical lordosis improvement does affect the long-term results of anterior cervical fusion with stand-alone cage for degenerative cervical disc disease: a retrospective study. Eur Spine J, 2012, 21: 1374–1382.

52. Njoku I, Alimi M, Leng LZ, Shin BJ, Hrtl R. Anterior cervical discectomy and fusion with a zero-profile integrated plate and spacer device: a clinical and radiological study: clinical article. J Neurosurg, 2014, 21: 529–537.

53. Chen Y, Wang X, Lu X, Yang L, Yang H, Yuan W. Comparison of titanium and polyetheretherketone (PEEK) cages in the surgical treatment of multilevel cervical spondylotic myelopathy: a prospective, randomized, control study with over 7-year follow-up. Eur Spine J, 2013, 22: 1539–1546.

54. Mac-Thiong JM, Labelle H, Roussouly P. Pediatric sagittal alignment. Eur Spine J, 2011, 20: 586.

55. Lou J, Liu H, Rong X, et al. Geometry of inferior endplates of the cervical spine. Clin Neurol Neurosurg, 2016, 142: 132–136.

56. Duval-Beaupère G, Schmidt C, Cosson P. A barycentremetric study of the sagittal shape of spine and pelvis: the conditions required for an economic standing position. Ann Biomed Eng, 1992, 20: 451–462.

57. Berthonnaud E, Dimnet JS, Roussouly P, Labelle H. Analysis of the sagittal balance of the spine and pelvis using shape and orientation parameters. J Spinal Disord Tech, 2005, 18: 40–47.